Friction riveting of 3D printed polyamide 6 with AA 6056-T6

dos Santos Mallmann, Paulo Henrique; Blaga, Lucian Attila; dos Santos, Jorge Fernandez; Klusemann, Benjamin

Published in:
Procedia Manufacturing

DOI:
10.1016/j.promfg.2020.04.319

Publication date:
2020

Document Version
Publisher's PDF, also known as Version of record

Available online at www.sciencedirect.com

ScienceDirect

Procedia Manufacturing 47 (2020) 406–412

Procedia MANUFACTURING

www.elsevier.com/locate/procedia

23rd International Conference on Material Forming (ESAFORM 2020)

Friction Riveting of 3D Printed Polyamide 6 with AA 6056-T6

Paulo Henrique dos Santos Mallmann[a], Lucian-Attila Blaga[a,*], Jorge Fernandez dos Santos[a], Benjamin Klusemann[a,b]

[a]*Institute of Materials Research, Materials Mechanics, Department of Solid State Joining Processes, Helmholtz-Zentrum Geesthacht, Geesthacht, Germany*
[b]*Institute of Product and Process Innovation, Leuphana University of Lüneburg, Lüneburg, Germany*

* Corresponding author. Tel.: +49 (0) 4152 87 2055. *E-mail address:* lucian.blaga@hzg.de

Abstract

Friction riveting (FricRiveting) is a technology for joining metallic and polymeric parts through frictional heat and pressure based on the principles of mechanical fastening and friction welding. Within this process, the joining occurs through the rotation of a metallic rivet, which is pressed onto a polymeric part while rotating at high speed, generating heat through the friction of the two materials, thus deforming and consequently anchoring the rivet inside the polymer. Compared to conventional joining techniques, FricRiveting has the advantages of fast joining cycles, no surface preparation or prior drilling required, and the joining can be produced single-sided. Without the presence of through-holes, the stress concentration is also minimized. This work aims to assess the feasibility and optimization of joining 3D printed Polyamide 6 (PA6) parts with AA6056-T6 rivets through FricRiveting. The feasibility is established by the occurrence of plastic deformation of the metallic rivet tip and thus formation of an anchor. The joint local mechanical properties are investigated via micro-hardness maps. Process temperature history recorded through infrared thermography is subsequently correlated with the joint formation and mechanical performance. The joint tensile strength was determined through pullout tests, which provided the results for the process validation and optimization through Box-Behnken and Full Factorial Design of Experiments, thus understanding the influence of FricRiveting parameters on the resulting properties of the joints.

Keywords: hybrid polymer-metal joints; friction riveting; design of experiments; joining by forming; 3D printing;

1. Introduction

Aluminum alloys, plastics and composites provide suitable solutions for overall weight reduction in the transportation industry. Well established solutions using aluminum alloys have been applied on engine, suspension, and interior parts, since they provide larger design freedom and have better corrosion resistance, but encounter some disadvantages because of the required welding processes, which increase the price of the final product [1], [2].

Polymers are key elements to achieve lightweight design in the automotive industry. Being used solely, or as matrix material of composites, they can replace metal parts, leading directly to a weight reduction. Together with their reduced mass, thermoplastic polymers bring additional advantages such as ease of manufacturing, design freedom, recyclability, resistance to abrasive environments or even noise reduction [3]. Polymers are currently used in seats, body panels, furnishings, lighting, reservoirs, among other parts within an automobile [3].

Among the thermoplastics used, polyamides are present in applications that require good heat stability, vibration resistance and resistance to coolant additives, like radiator tanks. Further examples include pedal boxes and engine covers. Nylon 6 (polyamide 6 or PA6) is synthesized by ring-polymerization from a ring-structured monomer called

10.1016/j.promfg.2020.04.319

caprolactam [4]. Each of its molecules contains six carbon atoms, thus, giving the name to the polymer produced. PA6 can be used for switches, mirror housings, fasteners, fuse boxes and cable ties. If the material is fiber-reinforced, PA6 is additionally used on door handles, fuel systems, wheel covers, among others [5]. This material has a good balance of mechanical properties, resistance to oil and chemical substances, wear and abrasion as well as long-term heat resistance (between 80 and 150 °C), high flexibility, low creep, high toughness and good resilience. It serves as a suitable composite matrix, as the strength and elastic modulus increase with fiber reinforcement. On the other hand, it is extremely hygroscopic, and the resistance to strong acids and bases is rather weak [3],[6], [7].

With the accessibility of additive manufacturing techniques, such as 3D printing, fabricating complete vehicle parts has become possible. 3D printing allows for a considerable range of variations in properties and material combinations, creating parts with application-tailored mechanical properties, as well as hybrid structures, with good dimensional accuracy at low cost [8]. The properties of 3D printed parts can be enhanced using nano- or fiber-reinforcements. Liu et al. [9] showed that reinforcing PA6 with carbon nanotubes increased its Young's modulus by over 200% and the yield strength by 160%, but at a price of a significant loss in ductility.

Replacing metallic with polymeric parts in the automotive sector takes place gradually, henceforth hybrid polymer-metal structures are increasingly designed. Joining metals and polymers is a significant challenge, due to the differences in physical-chemical properties of the two classes of materials. Regarding the methods currently used in industry, mechanical fastening is the most common choice [10]. Robust joints can be hereby produced, but with some restrictions, like reachability and double-sided access for some structures. Additionally, stress concentrations around the holes are present, which can weaken the joints. When applied in fiber-reinforced materials, mechanical fastening can end up weakening the composite due to fiber damage and further stress concentration [10]. Adhesive bonding is also an option for metal-polymer joining, consisting of an adhesive placed between two adherent surfaces, which solidifies, consolidating the joint [11]. It is a fair choice for dissimilar materials, as the adherents do not modify the microstructure of the connected materials, nor induce stress concentrations and, in case of composites, do not damage the fibers. On the other hand, adhesive joints are sensitive to the environment as well as to several solvents. As the adherents are polymers, temperature and humidity can have a significant influence on the joint properties. Extensive surface preparation are furthermore required, which ends up limiting the work time of the procedure, as for example, the preparation of aluminum for aerospace applications requires prior etching or anodization in acid solutions [12].

Friction riveting (FricRiveting) is an alternative technology for joining metal and polymeric parts through frictional heat and pressure. This process, patented at the Helmholtz-Zentrum Geesthacht [13], is based on friction welding and mechanical fastening. The joining occurs by rotating a metallic rivet, which is pressed onto a polymeric base plate at high rotational speed, generating heat through the friction of the two materials, thus deforming the rivet inside the polymer. Compared to other joining techniques, FricRiveting is advantageous due to its fast joining cycles, no surface preparation or prior drilling needed, no emissions and the joining is typically produced from one side, implying that only one-side access is required. As there are also no through-holes, stress concentration is also reduced [8] .

FricRiveting has been proven feasible for several material combinations, including several aluminum and titanium alloys, while the polymeric parts were either not reinforced or composite laminates. The process has been optimized for several material combinations, by statistical analysis and Design of Experiments [12].

Proenca *et al.* [14], [15], investigated the joinability of extruded PA6 with AA6056-T6 via FricRiveting. To the best of the authors' knowledge, this is the first time FricRiveting and generally friction based joining processes are investigated on 3D printed polymers.

2. Materials and Methods

2.1. Rivets

The solution heat-treated aluminum alloy AA6056-T6 was used for the rivets in this study. The tip of the rivets was drilled to produce the hole geometry presented in Fig. 1a. The microstructure, Fig. 1b, reveals grains aligned to the extrusion direction and a high number of inclusions related to the ingot casting process.

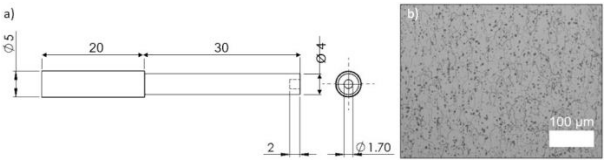

Fig. 1. AA6056-T6 rivet: (a) rivet geometry; (b) microstructure of base material.

2.2. 3D printing of the carbon fiber reinforced Polyamide 6

A commercial Mark Two 3D printer (MarkForged, USA) was used for producing the PA6 25x25x15 mm blocks. The extrusion temperature was 275°C and the printed layer thickness 0.175 mm. Since the PA6 filament is very hygroscopic, its spool needs to be dried at 80°C for 22 hours prior to the printing process. After drying, the filament is loaded into the 3D printer together with the carbon fiber filament, which is composed of 47% ±1% carbon fiber, embedded in a resin compatible to PA6. The actual fiber content corresponding to the amount of layers is thus shown in Table 1. The 3D printed CF-PA6 samples for the parameter screening and process optimization were produced with 100% fibers printed in an array of concentric rings.

Table 1. Correspondence of actual fiber content according to the fiber layer percentage in composite samples.

Amount of fiber layers	100%	50%
Actual fiber content	47% ±1%	23.5% ±0.5%

2.3. Friction Riveting

The process can be best described in its simplest variant, the metallic insert joint (also referred to as "point on plate joint"), shown in Figure 2. It is a forming-based joining technology, as the rotating cylindrical metallic rivet is deformed and anchored within a polymeric plate, because of heat accumulation due to the insulating thermal properties of the polymer.

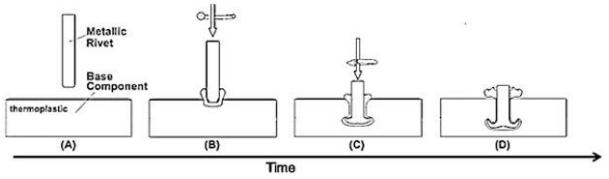

Fig. 2. Friction riveting process: (A) positioning of joining partners ; (B) rivet insertion into the polymer; (C) rivet plastic deformation / forging; (D) joint consolidation, reproduced from [12].

The joints in the present work were produced using a customized laboratory scale equipment (RNA, H. Loitz-Robotik, Hamburg, Germany). The feasibility for this material combination was investigated using a single-phased process variant with three parameters: rotational speed (RS), displacement at friction (DaF) and joining force (JF). This process variant has been described thoroughly by Proenca *et al.* [15], who observed that the rivet deformation can occur in some cases already in the friction phase for this material combination. The process is force controlled limited by displacement. The DaF corresponds to the spindle displacement of the welding head but cannot be correlated directly to the rivet insertion, as this is dependent on the polymer melting/softening. While the forging phase is not required for achieving rivet anchoring, a consolidation time is still recommended to avoid void formation related to differential contraction of the joined materials. Another single-phase process variant has been investigated by Cipriano *et al.*[16] , force-controlled limited by time. Time or displacement limitations can be useful in the FricRiveting process control to avoid full penetration of the polymeric parts, especially for this specimens or polymers with low melting point.

After an initial parameter screening (by a one-factor-at-a-time approach), the process was optimized through the Box-Behnken response surface design method (BBD). The parameter window investigated in this work is summarized in Table 2.

Table 2. Friction riveting process parameter window for BBD response surface method.

Level	Rotational Speed [rpm]	Displacement at Friction [mm]	Joining Force [N]
-1	19000	7	1500
0	20000	9	2000
1	21000	11	2500

The design generated 15 samples (performed and tested in randomized order) with three center points (replicated conditions). For validation, three additional joining conditions have been produced within the tested parameter range. The parameter combinations for the 15 samples are shown in Table 3.

Table 3. Design of Experiments (Box-Behnken scheme). RS: rotational speed; DaF: displacement at friction; JF: joining force.

Sample	RS [rpm]	DaF [mm]	JF [[N]
1	21000	7	2000
2	20000	9	2000
3	20000	9	2000
4	20000	9	2000
5	19000	9	1500
6	20000	11	2500
7	19000	7	2000
8	21000	11	2000
9	19000	9	2500
10	20000	7	2500
11	21000	9	1500
12	20000	7	1500
13	20000	11	1500
14	19000	11	2000
15	21000	9	2500

Joint formation was assessed by micro-computed tomography (μCT) prior to tensile testing, while fracture mode analysis was performed by cutting cross sections through the centre of the failed joints, which were evaluated via optical microscopy (Keyence VHX-6000).

2.4. Process temperature evolution

The temperature development during the process was measured by infrared thermography on the expelled polymeric flash material, using an Image IR8800 (InfraTec, Germany) infrared camera. Due to the large temperature variations expected during the process, a combined 150°C-700°C filter was used. The data was processed with the IRBIS 3 software.

2.5. Mechanical properties and behavior

Local mechanical properties were evaluated via Vickers microhardness mapping for both rivet base material and joints. The global mechanical performance was investigated by means of ultimate tensile force (UTF), using a universal testing machine (100 kN load cell, Zwick Roell, Germany) at room temperature at a traverse speed of 1 mm/min. The mentioned T-pull tensile testing and clamping system is the

same used for the previous works on FricRiveting and has been described in detail in [12].

3. Results

3.1. Joint formation and optimization through BBD response surface methodology

Figure 3 shows the values of the ultimate tensile force (UTF) for the 15 samples according to the DoE plan in Table 3.

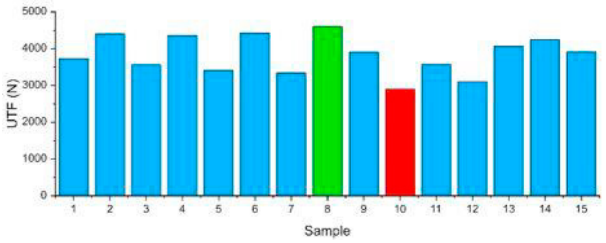

Fig. 3. Ultimate tensile force (UTF) of the BBD experiments, see Table 3. Sample 8 (marked green) resulted in the maximum UTF and Sample 10 (marked red) the minimum UTF obtained, respectively.

In order to determine the effect of each process parameter and especially the second order interactions on the rivet anchoring and consequently UTF, corresponding contour plots have been generated and correlated to the obtained rivet anchoring, see Figs. 4-6. For each specific region, one parameter set (sample) is displayed which led to a low anchoring (I) or high anchoring efficiency (II).

The optimal combination for the investigated parameter range based on the response surface design is determined as: RS 21000 rpm, DaF 11 mm and JF 2200 N. From Fig. 4 one can observe that the UTF increases with increasing RS and DaF. A RS of 21000 rpm represents the maximum capacity of the employed equipment. An increase of DaF above 11 mm is only possible by changing the initial length of the rivet (currently 50 mm, where 20 mm are clamped inside the welding head, see Fig. 1), as otherwise there is a high risk of collision between spindle and polymeric plate.

Figure 7 displays the joint formation and failure modes for the runs with the maximum (condition 8) and minimum (condition 10) UTF, respectively.

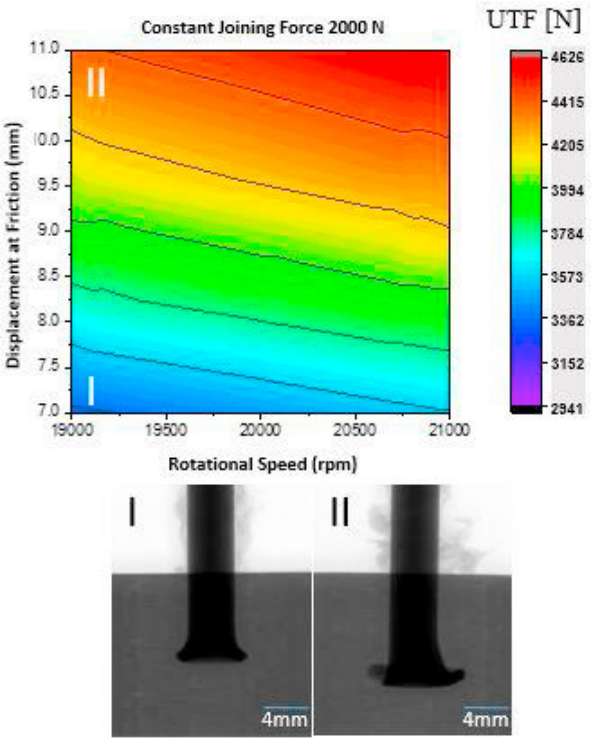

Fig. 4. Contour plot at constant joining force of 2000 N. Regions of minimum (I) and maximum (II) UTF are identified. The corresponding µCT displaying the joint formation for one sample in each region are shown below.

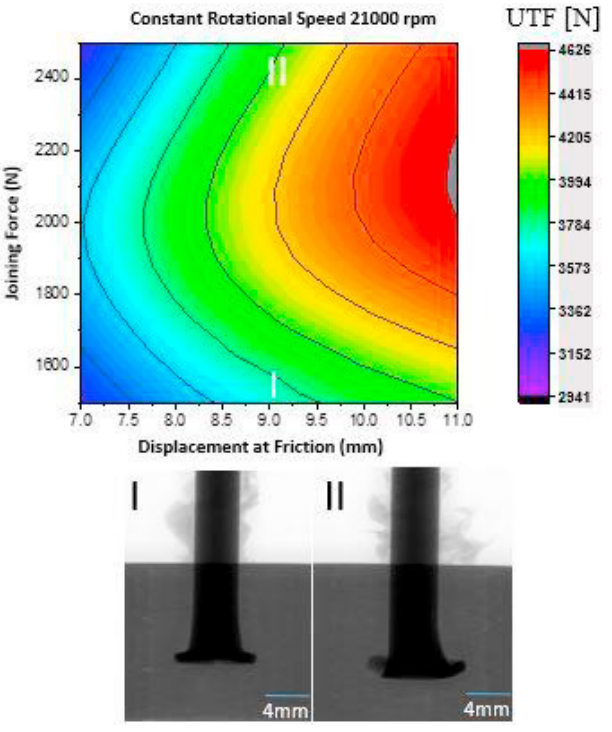

Fig. 5. Contour plot at constant rotational speed of 21000 rpm. Regions of minimum (I) and maximum (II) UTF are identified. The corresponding µCT displaying the joint formation for one sample in each region are shown below.

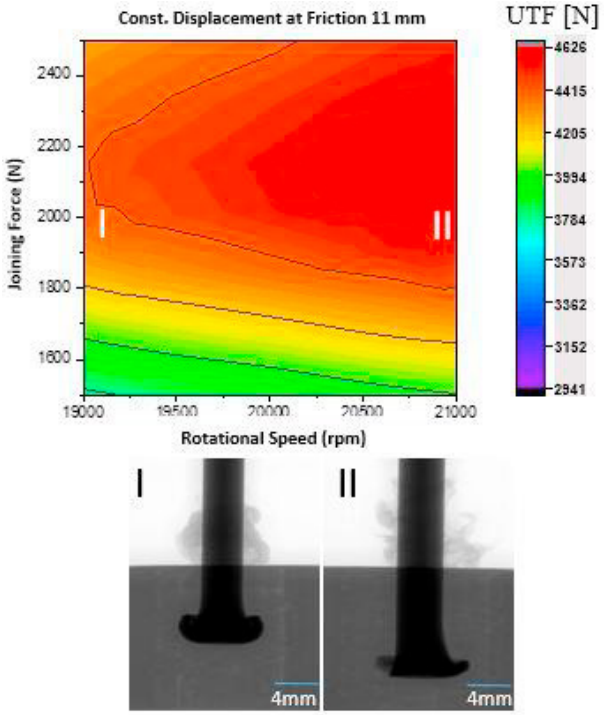

Fig. 6. Contour plot at constant Displacement at Friction of 11 mm. Regions of minimum (I) and maximum (II) UTF are identified. The corresponding µCT displaying the joint formation for one sample in each region are shown below.

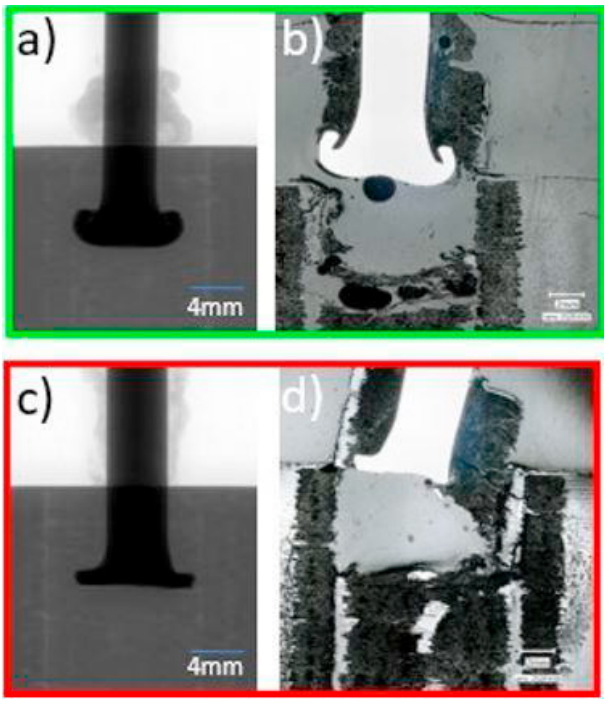

Fig. 7. µCT and corresponding fracture image after tensile testing for experimental Sample 8 (a,b) and 10 (c,d).

For the process conditions leading to the lowest mechanical performance in terms of UTF, failure through the leg of the deformed rivet shape is observed, Fig. 7d). This behavior, which was also observed by Proenca *et al.* [15] and Cipriano *et al.* [17], is explained by the reduced cross section of the deformation legs. Rivets with a large tip deformation provide sufficient anchoring within the polymer, but can nonetheless lead to premature failure, if the deformed rivet legs are too thin. This was even more prone to occur in the present case, as the rivet tip was machined by hole drilling, as described in Section 2.1.

The optimal condition was tested, to verify the consistency of the prediction, as the BBD does not consider replicates, along with three additional validation conditions, Table 4. The validation plot is presented in Figure 8.

Table 4. Based on BBD determined optimal condition and validation conditions

Condition	RS [rpm]	DaF [mm]	JF [N]
Optimal	21000	11	2200
Validation 1	21000	11	2500
Validation 2	19000	7	1500
Validation 3	20000	9	2500

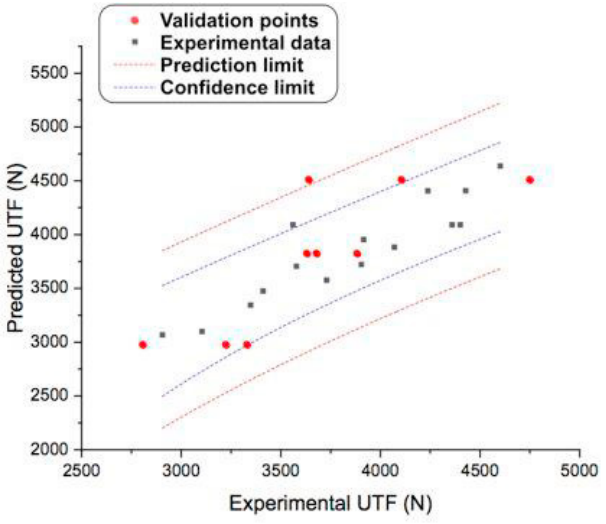

Fig. 8. Validation plot of the BBD response surface predicted vs experimental UTF.

The R^2 of the prediction model for the UTF is 83.4, with a standard deviation of 278.4 N. The UTF prediction is made using the generated regression equation (1), at the confidence interval of 95%:

$$UTF = -6644 + 0.1156 \cdot RS + 4.35 \cdot DaF + 5.02 \cdot JF - 0.00249 \cdot DaF^2 - 0.001507 \cdot JF^2 + 0.00139 \cdot DaF \cdot JF \quad (1)$$

The UTF of the optimal condition is predicted as 4670 N, while the experimental value was 4885 N, which lies within the predicted standard deviation. The obtained experimental UTF was 91% of the tested rivet ultimate tensile force (5370 N ± 200 N). The joint failed through tensile failure in the shaft

of the metallic rivet. The reason for the slight underestimation of the mechanical properties might be related to the exposure to heat and consequent reduction of microhardness for T6 tempered alloys. Figure 9 shows the joint formation, fracture mode and microhardness distribution for the optimized process parameters.

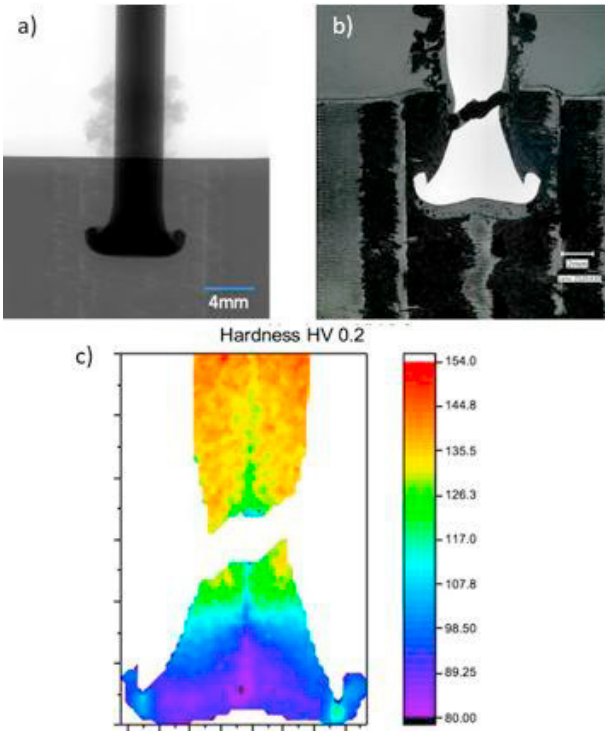

Fig. 9. Joint produced with determined optimal joining parameter: a) µCT image of the joint; b) failure mode through the metallic rivet; c) microhardness map showing failure occurring in the region with decreased local mechanical properties (HV in failure region lower than base material).

The underestimation of the properties due to heat treatment and loss of the T6 tempering is confirmed by the process temperature evolution measurement, see Figure 10. Infrared thermography revealed a peak temperature of 379°C, which is at around 60% of the typical aluminum melting point. At this level of temperature exposure in friction stir based processing, heat treatable alloys such as AA6056-T6 suffer metallurgical transformations, like dissolution of precipitates, and inherent reduction of mechanical properties [18].

Further microstrostructural investigations as well as thermal analyzes need to be performed in order to confirm the actual metallurgical transformation causing the reduction of mechanical properties due to friction riveting in this combination of material, which is not within the scope of the present work.

As mentioned in Section 2.2, the BBD optimization was performed on 3D printed PA6 samples with 100% fiber content. The 100% fiber content is not efficient in terms of material usage and further optimization is required as well to produce the composite joining partner.

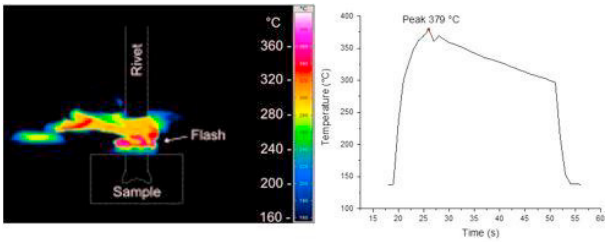

Fig. 10. Infrared thermography of the process temperature development during friction riveting. Maximum temperature measured on the expelled polymeric flash material was 379°C.

The identified optimal process condition for 100% fiber content PA6 has been further applied on a 50% fiber layer printed at 0°/90° orientation. Usage of 50% fiber layer reduces the overall material consumption significantly, concentrating the carbon fiber array around the rivet shaft and the rivet anchoring zone. T-pull tests of this exploratory condition resulted in an average UTF of 4650 N and a failure through the breaking of the deformation legs, as shown in Figure 11. These preliminary results indicate a similar mechanical performance in terms of UTF as for the 100% fiber content friction riveted samples, despite different failure modes. This means that the tested fiber array provides sufficient reinforcement of the anchoring zone to withstand a similar load as the 100% fiber content samples, at a lower fiber material consumption.

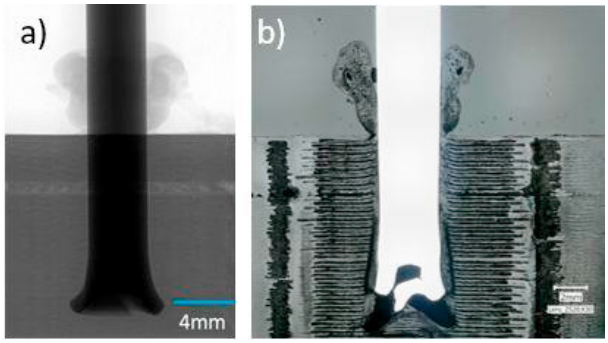

Fig. 11. Previously identified optimal process conditions applied on 50% fiber content 3D printed CF-PA6: a) µCT image of the joint; b) failure mode through breaking of a deformation leg in the metallic rivet.

4. Conclusions

The current work successfully investigated the joinability of friction riveting on additive manufacture polymeric composites. A single-phased process variant controlled by force and limited by spindle displacement was optimized via Box-Behnken response surface methodology. AA6056-T6 were successfully joined with 3D printed carbon fiber reinforced PA6, with the optimal condition reaching over 90% of the base material strength and failure through the metallic rivet. Maximum temperatures of around 60% of the melting point of aluminum were measured during the process, leading most likely to a loss of the T6 tempering state, which

consequently leads to a decrease in microhardness and tensile strength of the rivet.

3D printed carbon-fiber reinforced thermoplastic was proven feasible to be joined via friction riveting in hybrid polymer-metal structures and optimized for a 100% fiber content. Moreover, it was shown that even reducing the fiber content to half, similar ultimate tensile strengths can be achieved. Further optimization of the 3D printing process with regard of locally strengthening of the anchoring zone of friction riveted joints is required. This can provide the basis for further tailoring of joining areas and anchoring zones and extend the area of applicability of the friction riveting process to 3D printed materials, as well as further increase the joint mechanical performance within the current limits of the technique by locally manipulating the anchoring material properties.

Further work will investigate the microstructural changes in both AA6056 and CF-PA6 and correlate it with the 3D printing and friction riveting processing conditions in order to understand the joint formation in additive manufactured parts more thoroughly.

References

[1] Luo AA. Magnesium: Current and potential automotive applications. JOM 2002; 54(2):42–8.
[2] Hovorun TP, Berladir KV, Pererva VI, Rudenko SG, Martynov AI. Modern materials for automotive industry. J. Eng Sci 2017: 4(2):f8–f18.
[3] Crompton TR. Engineering Plastics. Smithers Rapra; 2014.
[4] Harper CA. Handbook of plastics, elastomers & composites. 4th ed. New York: McGraw-Hill; 2002.
[5] Wypich G. Handbook of polymers. Toronto: ChemTec Publishing; 2012.
[6] McKeen LW. Film Properties of Plastics and Elastomers. 4th ed. Amsterdam: Elsevier; 2017.
[7] Engkvist G. Investigation of microstructure and mechanical properties of 3D printed Nylon. Luleå University of Technology, Sweden, 2017.
[8] Wang X, Jiang M, Zhou Z, Gou J, Hui D. 3D printing of polymer matrix composites: A review and prospective. Compos Part B Eng 2017; 110:442–458.
[9] Liu T, Yee Phang I, Shen L, Yin Chow S, Zhang WD. Morphology and Mechanical Properties of Multiwalled Carbon Nanotubes Reinforced Nylon-6 Composites. Macromolecules 2004; 37:7214–7222.
[10] Chaves CE, Inforzato DJ, Fernandez FF. Principles of Mechanical Fastening in Structural Applications. In Joining of polymer-metal hybrid structures: principles and applications. Amancio-Filho ST and Blaga LA. Eds. Hoboken, NJ: John Wiley & Sons Inc; 2017. 147–185.
[11] Dorworth LC, Dillingham G. Fundamentals of adhesive bonding of composite materials. AeroDef Manufacturing, Fort Worth TX, March 6, 2017.
[12] Amancio-Filho ST, Blaga LA. Joining of polymer-metal hybrid structures : principles and applications. Eds. Hoboken, NJ: John Wiley & Sons Inc; 2018.
[13] Amancio-Filho ST, Beyer M, dos Santos JF. US 7,575,149 B2. Method of connecting a metallic bolt to a plastic workpiece. US patent; 2009.
[14] Proença BC, Blaga LA, dos Santos JF, Canto LB, Amancio-Filho ST. Force controlled friction riveting of glass fiber reinforced polyamide 6 and aluminum alloy 6056 hybrid joints. In Proc. ANTEC 2015. Orlando FL, March 23-25, 2015.
[15] Proença BC, Blaga LA, dos Santos JF, Canto LB, Amancio-Filho ST. Friction riveting ('FricRiveting') of 6056 T6 aluminium alloy and polyamide 6: influence of rotational speed on the formation of the anchoring zone and on mechanical performance. Weld Int 2017; 31(7):509-518.
[16] Cipriano GP, Ahiya A, dos Santos JF, Vilaça P, Amancio-Filho ST. Single-phase friction riveting: metallic rivet deformation, temperature evolution, and joint mechanical performance. Weld World 2019; 64:47-58.
[17] Cipriano GP, Blaga LA, dos Santos JF, Vilaça P, Amancio-Filho ST. Fundamentals of force-controlled friction riveting: Part II-Joint global mechanical performance and energy efficiency. Materials (Basel) 2018; 11(12):2489.
[18] Gallais C, Denquin A, Bréchet Y, Lapasset G. Precipitation microstructures in an AA6056 aluminium alloy after friction stir welding: characterisation and modelling. Mater Sci Eng A 2008; 496:77–89.